Cross sections and rates for direct electron-impact ionization of sodiumlike ions

S. M. Younger
National Bureau of Standards, Washington, D. C. 20234
(Received 6 March 1981)

Cross sections and rate coefficients for the direct electron-impact ionization of sodiumlike ions have been calculated in a distorted-wave Born exchange approximation. For higher charge states the cross section is dominated by inner-shell ionization of the $2p^6$ subshell. Analytic fits to the data allow rapid calculation of cross sections and rate coefficients over a wide range of incident electron energies. The importance of electron-impact excitation to autoionizing states is discussed.

I. INTRODUCTION

Electron-impact-ionization cross sections are important components in the modeling and diagnostics of high-temperature plasmas, both laboratory and astrophysical. Until recently, however, very little quantitative information was available on ionization cross sections and rates for highly ionized atoms. Measurements in plasma devices such as theta pinches[1] have yielded information only on total ionization rates at isolated electron temperatures and are thus difficult to compare to other experiments and theoretical calculations which study ionization from specific energy levels within the ion. Cross-beam experiments measure individual state cross sections but are difficult to perform on highly charged species.[2]

Theoretically, electron-impact ionization is a formidable problem due to the double continuum electron final state. Various methods based on the Born approximation have been applied with reasonable success to simple ions in the hydrogen-through-boron isoelectronic sequences,[3-7] although it must be noted that reliable experimental data for comparison purposes are available only for a few ions.

The present paper reports the results of electron-impact-ionization cross-section calculations for several sodiumlike ions (Mg II, Al III, P V, Ar VIII) based on a distorted-wave Born exchange approximation. Section II gives a brief description of the method employed. Section III presents the results compared to other theoretical and experimental data. Section IV is a discussion, with particular attention given the importance of inner-shell ionization, both by direct electron impact and by autoionization of discrete electron-impact excited states above the ion limit.

II. METHOD

A detailed description of the distorted-wave Born exchange approximation employed here has been given elsewhere.[6-8] Briefly, the scattering matrix is expressed in terms of a triple partial-wave expansion, one initial state and two final-state continua, with the phase of the exchange matrix element chosen so as to maximize the exchange-interference term and thus minimize the total cross section within the Born exchange approximation. The incident distorted waves were generated in a local energy-dependent potential consisting of the direct terms of the frozen-core Hartree-Fock potential of the target ground state plus a semiclassical exchange potential approximation:

$$V^N = -\frac{Z}{r} + 2J_{1s} + 2J_{2s} + 6J_{2p} + J_{3s} + V^N_{\rm SCE}\,, \qquad (1)$$

where

$$J_i(r) = \frac{1}{r}\int_0^r [P_i(\rho)]^2 d\rho + \int_r^\infty \frac{[P(\rho)]^2}{\rho}\, d\rho \qquad (2)$$

is the electrostatic potential associated with the ith orbital with radial part $P_i(r)$. Z is the nuclear charge and $V^N_{\rm SCE}$ is a semiclassical exchange potential for N electrons[9]:

$$V^N_{\rm SCE}(r) = \frac{E - V^N_D}{2} - \tfrac{1}{2}[(E - V^N_D)^2 + \alpha^2]^{1/2}, \qquad (3)$$

where

$$\alpha^2 = \frac{2}{r^2}\sum_{i=1}^{N} [P_i(r)]^2 \qquad (4)$$

and

$$V^N_D = V^N - V^N_{\rm SCE}\,. \qquad (5)$$

In the direct scattering matrix element the ejected (lower-energy) electron and the final (higher-energy) electron partial waves were computed in the potentials V^{N-1} and V^N, respectively, where

$$V^{N-1} = -\frac{Z}{r} + 2J_{1s} + 2J_{2s} + 6J_{2p} + V^{N-1}_{\rm SCE}, \qquad (6)$$

with $V^{N-1}_{\rm SCE}$ the semiclassical exchange potential omitting the $3s$ ionized electron. In the exchange matrix element the potentials for the ejected and final scattered partial waves were reversed, with the lower-energy ejected wave computed in V^N and the higher-energy scattered wave computed in V^{N-1}. Such an arrangement assures orthogonality between overlapping partial waves in the scattering matrix element. For inner-shell ionization from the $2p$ and $2s$ subshells the potentials are the same except that V^{N-1} omits the appropriate $n=2$ orbital instead of the $3s$.

Distorted waves were generated numerically over a 350-point block linear radial grid. For incident electron energies less than or equal to $1.5I$, where I is the subshell ionization energy, the maximum partial-wave angular momenta included for the incident, ejected, and final waves were 10, 6, and 10, respectively. For incident electron energies greater than $1.5I$ the maxima were increased to 15, 10, and 15, respectively. At five times threshold, the highest incident electron energy considered, an extrapolation over higher incident wave partial angular momenta was required, although it amounted to only a few percent of the total cross section. The integration over the final-state partial-wave energy distribution was accomplished with three-point and five-point Gauss-Legendre formulas in the low- and high-energy ranges, respectively.

Ground-state Hartree-Fock wave functions from the tabulation of Clementi and Roetti[10] were employed for the target. Table I lists the ionization energies. Experimental energies were used where they are available.

TABLE I. Ionization energies (eV) for sodiumlike ions.

Ion/subshell	$3s$	$2p$	$2s$
Mg II	15.035[a]	68.050[b]	111.2[e]
Al III	28.447[a]	105.24[c]	153.8[e]
P V	65.023[a]	201.18[d]	260.4[e]
Ar VIII	143.46[a]	396.72[d]	472.4[e]

[a] Reference 18.
[b] Reference 19.
[c] Reference 20.
[d] Reference 21.
[e] Reference 10.

III. RESULTS

Electron-impact-ionization cross sections for Mg II, Al III, P V, Ar VIII, and the $Z=\infty$ limit computed in the distorted-wave Born exchange approximation described above are given in Table II. In order to suppress the gross Z dependence of the cross section we tabulate the classically scaled cross section uI^2Q, where $u=E/I$ is the incident electron's energy in ionization threshold units, I is the ionization energy in eV, and Q is the cross section in cm^2. For the purpose of comparison, distorted-wave cross sections neglecting electron exchange in the scattering matrix element are given in parentheses.

TABLE II. Scaled electron-impact-ionization cross sections uI^2Q for highly ionized sodiumlike ions in units of 10^{-14} cm^2 eV^2.

u_{3s}	Mg II	Al II	P V	Ar VIII	$Z=\infty$
	$1s^22s^22p^63s \to 1s^22s^22p^6+e^-$				
1.125	0.527 (0.505)[a]	0.462 (0.435)	0.446 (0.412)	0.485 (0.449)	0.592 (0.506)
1.25	0.944 (0.955)	0.831 (0.821)	0.817 (0.793)	0.890 (0.863)	1.07 (0.966)
1.50	1.57 (1.70)	1.41 (1.49)	1.43 (1.48)	1.54 (1.59)	1.83 (1.78)
2.25	2.71 (3.19)	2.53 (2.92)	2.62 (2.99)	2.83 (3.19)	3.31 (3.60)
3.50	3.77 (4.49)	3.62 (4.30)	3.80 (4.45)	4.12 (4.79)	4.76 (5.40)
5.00	4.51 (5.38)	4.37 (5.18)	4.67 (5.45)	5.03 (5.83)	5.70 (6.51)
	$1s^22s^22p^63s \to 1s^22s^22p^53s+e^-$				
1.125	0.905 (0.761)	1.79 (1.53)	3.01 (2.55)	3.70 (3.10)	4.43 (3.61)
1.25	2.09 (1.89)	3.74 (3.39)	5.80 (5.17)	6.93 (6.11)	8.03 (6.90)
1.50	4.99 (4.87)	7.79 (7.57)	10.8 (10.4)	12.4 (11.8)	13.7 (12.7)
2.25	14.8 (15.4)	19.2 (20.1)	23.0 (24.0)	24.6 (25.6)	24.4 (25.4)
3.50	28.8 (30.8)	33.7 (36.4)	37.1 (40.2)	37.8 (41.1)	34.2 (37.9)
5.00	41.0 (44.1)	46.0 (49.7)	48.4 (52.7)	48.0 (52.5)	41.0 (46.5)
	$1s^22s^22p^63s \to 1s^22s2p^63s+e^-$				
1.125	0.288 (0.271)	0.474 (0.463)	0.727 (0.708)	0.873 (0.834)	1.15 (1.03)
1.25	0.699 (0.684)	1.00 (1.04)	1.41 (1.44)	1.65 (1.65)	2.11 (1.99)
1.50	1.58 (1.73)	2.10 (2.32)	2.68 (2.89)	3.03 (3.19)	3.67 (3.69)
2.25	4.41 (5.07)	5.12 (5.90)	5.80 (6.64)	6.18 (7.02)	6.83 (7.55)
3.50	8.09 (9.31)	8.86 (10.2)	9.46 (11.0)	9.74 (11.3)	9.95 (11.4)
5.00	11.1 (12.6)	11.8 (13.5)	12.4 (14.2)	12.5 (14.4)	12.3 (14.0)

[a] Numbers in parentheses are distorted-wave no-exchange values.

Figure 1 is a Fano plot of the present results for Mg II compared to the experimental data of Martin *et al.*[11] and to other theoretical calculations. The distorted-wave cross sections are about 10% above a fit to the experimental points.

In order to facilitate the interpolation and extrapolation of the present data for sodiumlike ions, we have fit the distorted-wave Born exchange cross sections of Table II by the formula

$$uI^2Q = A\left(1-\frac{1}{u}\right)+B\left(1-\frac{1}{u}\right)^2+C\ln u+\frac{D}{u}\ln u, \quad (7)$$

where A, B, C, and D are Z-dependent parameters given by the inverse power series

$$A=\sum_{n=0}^{3}\frac{a_n}{(Z-10)^n},\qquad B=\sum_{n=0}^{3}\frac{b_n}{(Z-10)^n}, \quad (8)$$

etc. The parameters A, B, and D were determined by a fit to the distorted-wave cross sections.[12] The parameter C is a Bethe coefficient governing the high-energy behavior of the cross section, and is given by

$$C=\frac{I}{\pi\alpha}\int_I^\infty \frac{\sigma}{\epsilon}\,d\epsilon, \quad (9)$$

where σ is the photoionization cross section and α is the fine-structure constant. Photoionization cross sections used to compute the Bethe parameter C were taken from the tabulations of Manson.[13] Table III lists the coefficients a_n, b_n, c_n, d_n which reproduce the data of Table II to within a few percent.

By averaging Eq. (7) over a Maxwellian velocity distribution for the incident electron energy one may derive an expression for the electron-impact-ionization rate coefficient S (in cm^3/sec) as a correction to the commonly used Seaton semiempirical formula[14]

$$S^{\mathrm{Seaton}}=2.2\times10^{-6}\sqrt{\chi}\,I^{-3/2}e^{-1/\chi}, \quad (10)$$

where I is the individual subshell ionization energy in eV and χ is the reduced electron temperature

$$\chi = kT/I. \quad (11)$$

The distorted-wave rate coefficient is then

$$S^{\mathrm{DW}}=F(\chi)S^{\mathrm{Seaton}}, \quad (12)$$

where $F(\chi)$ is a distorted-wave factor given by

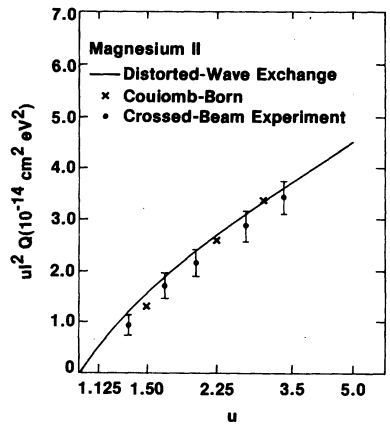

FIG. 1. Fano plot of the scaled electron-impact-ionization cross section for Mg II below the threshold for inner-shell ionization. ——, distorted-wave Born exchange approximation; ×, Coulomb-Born, no exchange, Ref. 15; •, crossed-beam experiment, Ref. 11.

$$F(\chi)=\frac{3.0\times10^{13}}{\chi}\left(\left[A+B\left(1+\frac{1}{\chi}\right)\right]+\left\{C-\frac{1}{\chi}\left[A+B\left(2+\frac{1}{\chi}\right)\right]\right\}\alpha(\chi)+\frac{D}{\chi}\beta(\chi)\right), \quad (13)$$

with

$$\alpha(\chi)=\frac{0.001\,93+0.9764\chi+0.6604\chi^2+0.025\,90\chi^3}{1.0+1.488\chi+0.2972\chi^2+0.004\,925\chi^3} \quad (14)$$

and

$$\beta(\chi)=\frac{-0.000\,572\,5+0.013\,45\chi+0.8691\chi^2+0.034\,04\chi^3}{1.0+2.197\chi+0.2457\chi^2+0.002\,053\chi^3}. \quad (15)$$

IV. DISCUSSION

As the nuclear charge increases along the sodium isoelectronic sequence the total cross sections for electron-impact ionization at intermediate and high-incident electron energies become dominated by inner-shell processes. There are two principal reasons for this behavior. First, for higher charge states the thresholds for ionization of the inner subshells decrease relative to the valence electron ionization energy. For example,

TABLE III. Parameters for the isoelectronic fit of the distorted-wave Born exchange electron-impact-ionization cross sections for sodiumlike ions (10^{-14} cm^2 eV^2).

	$i=0$	1	2	3
$a_i(3s)$	9.86	−20.0	92.4	−92.2
$b_i(3s)$	−3.20	13.4	−69.7	75.5
$c_i(3s)$	1.06	−1.39	−2.95	5.29
$d_i(3s)$	−5.65	7.69	−47.6	54.5
$a_i(2p)$	79.1	23.3	−463.0	670.0
$b_i(2p)$	−24.8	−62.5	422.0	−644.0
$c_i(2p)$	5.18	96.8	−203.0	170.0
$d_i(2p)$	−44.6	−158.0	416.0	−463.0
$a_i(2s)$	18.1	95.5	−444.0	538.0
$b_i(2s)$	−4.95	−64.3	324.0	−403.0
$c_i(2s)$	2.68	5.28	−13.7	10.5
$d_i(2s)$	−10.7	−118.0	433.0	−497.0

for Mg II, $I_{2p}/I_{3s}=4.52$ and $I_{2s}/I_{3s}=7.39$, while for Ar VIII $I_{2p}/I_{3s}=2.75$ and $I_{2s}/I_{3s}=3.29$. The second reason for the increased importance of inner-shell processes for high charge states is the isoelectronic scaling of the inner-shell cross section. Figure 2 is an isoelectronic plot of the scaled electron-impact-ionization cross sections for sodiumlike ions. Each curve represents a fixed incident-electron energy measured in units of I_{3s}. Total cross sections including both valence and inner-shell direct ionization are shown as solid curves. Cross sections for $3s$ ionization only are shown by dashed curves for $u_{3s}=3.5$ and 5.0. From Fig. 2 and Table II it is apparent that while the scaled ionization cross section for $3s$ ejection does not vary significantly versus the nuclear charge, the $2p$ inner-shell cross section increases by almost a factor of 4 at $u=1.125$ from Mg II to Ar VIII. This breakdown in classical scaling by the square of the ionization energy is analogous to a similar situation found in the Ne sequence. As the incident energy increases the deviation from classical scaling of the $2p$ cross section decreases, so that at $u=5$, uI^2Q varies by less than 25% between Mg II and Ar VIII. Thus, near the $2p$ threshold one finds a much larger relative contribution to the total cross section for more highly ionized atoms. Figure 3 is a comparison of the total cross sections for direct electron-impact ionization of Mg II and Ar VIII, clearly demonstrating the increased importance of inner-shell ionization.

In addition to the direct ejection of target electrons by electron impact, one must consider the contribution to the total effective ionization cross section due to autoionization of excited states above the ionization limit of the ion. Such states, which are actually resonances in the ejected-electron continuum, have substantial electron-excitation cross sections which increase rapidly with Z relative to the valence-electron direct-ionization cross section. Consideration of this indirect ionization mechanism is complicated by the complex configuration interaction and intermediate coupling affecting such states as well as

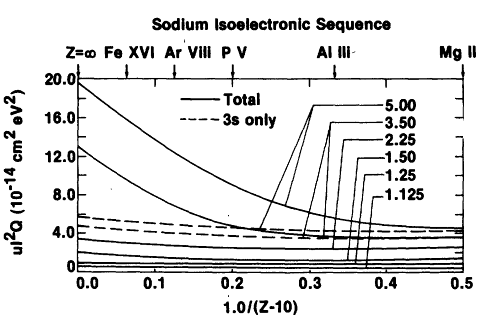

FIG. 2. Isoelectronic plot of the total cross sections for direct electron-impact ionization of sodiumlike ions computed in the distorted-wave Born exchange approximation. Each curve represents the cross section at a given incident electron energy in units of the $3s$ ionization energy. The cross sections for ionization of the $3s$ valence electron, ignoring inner-shell contributions, are given as dashed lines.

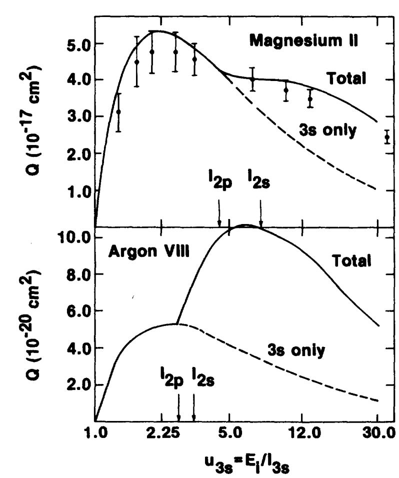

FIG. 3. Comparison of the total cross sections for direct electron-impact ionization of Mg II and Ar VIII, illustrating the importance of inner-shell ionization at high charge states. ●, crossed-beam experiment, Ref. 11.

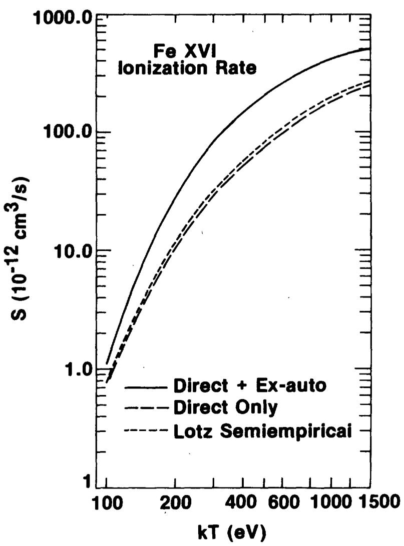

FIG. 4. Electron-impact ionization-rate coefficient versus electron temperature for Fe XVI, comparing the contributions due to direct ionization (present results) with those due to ionization via excitation to autoionizing states, Ref. 16.

the necessity to consider nonunit branching ratios for autoionization versus radiative stabilization to nonautoionizing levels. For Mg II, where almost all of the ions in levels above the $3s$ ionization limit are expected to autoionize, Moores and Nussbaumer[15] calculate a 25% increase in the total ionization cross section due to excitation to autoionizing states. For Fe XVI, however, Cowan and Mann[16] have demonstrated that the excitation-autoionization mechanism is the dominant contribution to the total effective ionization rate in the near-threshold electron-temperature region even though a substantial fraction of the excited states decay radiatively to nonautoionizing bound states. As the nuclear charge is increased still further, Cowan and Mann estimate that the relative contribution of excitation-autoionization to the total effective ionization rate will remain approximately the same since the mechanism will be dominated by excitation to levels which are stable against radiative decay and which have excitation cross sections scaling smoothly with Z. Figure 4 plots the total effective ionization rate of Fe XVI, including the excitation-autoionization contribution calculated by Cowan and Mann. Also shown in Fig. 4 is the prediction of the semiempirical formula of Lotz,[17] which is in good agreement with the direct ionization rate, but not the total rate including excitation-autoionization mechanisms.

Note that ejection of a $2s$ or $1s$ orbital leaves a sodiumlike ion in an autoionizing configuration, resulting in effective double ionization by a single electron impact. The small ionization cross sections associated with these subshells, however, suggest only a minor role for such double-ionization events. We have not calculated ionization cross sections for the $1s$ subshell. Reasonable estimates of K-shell ionization cross sections may be obtained from data on He-like ions.[7]

It is difficult to assess the accuracy of the present calculations for direct electron-impact-ionization cross sections of sodiumlike ions. Although good agreement between theory and crossed-beam experiment was found for Mg II, further comparisons are required in order to establish the isoelectronic scaling of the total cross section. Although one expects that simple independent-particle methods will become more accurate as the nuclear charge dominates the electrostatic interaction, it is not clear how rapid and in what form this convergence will be manifested.

ACKNOWLEDGMENTS

I would like to thank S. Manson for making available his extensive tabulations of theoretical photoionization cross sections which were used in the computation of the Bethe parameters. This work was supported in part by the U. S. Department of Energy.

[1] W. L. Rowan and J. R. Roberts, Phys. Rev. A 19, 90 (1979).
[2] K. T. Dolder and B. Peart, Rep. Prog. Phys. 39, 693 (1976).
[3] L. B. Golden and D. H. Sampson, J. Phys. B 10, 2229 (1977).
[4] D. L. Moores, J. Phys. B 5, 286 (1972).
[5] E. Stingl, J. Phys. B 5, 1160 (1972).
[6] S. M. Younger, Phys. Rev. A 22, 111 (1980).
[7] S. M. Younger, Phys. Rev. A 22, 1425 (1980).
[8] S. M. Younger, Phys. Rev. A 23, 1138 (1981).
[9] M. E. Riley and D. G. Truhlar, J. Chem. Phys. 63, 2181 (1975).
[10] E. Clementi and C. Roetti, At. Data Nucl. Data Tables 14, 177 (1974).
[11] S. O. Martin, B. Peart, and K. T. Dolder, J. Phys. B 1, 537 (1968).
[12] S. M. Younger (unpublished).
[13] S. Manson (private communication).
[14] M. J. Seaton, Planet. Space Sci. 12, 55 (1964).
[15] D. L. Moores and H. Nussbaumer, J. Phys. B 3, 161 (1970).

[16]R. D. Cowan and J. B. Mann, Astrophys. J. 232, 940 (1979).

[17]W. Lotz, Z. Phys. 216, 241 (1968).

[18]C. E. Moore, *Ionization Potentials and Ionization Limits*, National Stand. Ref. Data Ser. (National Bureau of Standards, Washington, D. C., 1970), No. 34.

[19]W. C. Martin and R. Zalubas, J. Phys. Chem. Ref. Data 9, 1 (1980).

[20]W. C. Martin and R. Zalubas, J. Phys. Chem. Ref. Data 8, 817 (1979).

[21]C. E. Moore, *Atomic Energy Levels*, National Stand. Ref. Data Ser. (National Bureau of Standards, Washington, D. C., 1971), Vol. 1, No. 35.